Postfire seismic performance of reinforced precast concrete columns

Ugur Demir, Mark F. Green, and Alper Ilki

- This paper explores the lateral load capacity and seismic performance of reinforced precast concrete columns that have been damaged by fire.
- Full-scale precast concrete columns were subjected to fires of various duration and tested to determine the impact of fire damage on force-displacement behavior, moment-curvature relationship, stiffness, energy dissipation capacity, and residual displacements.
- Analytical models were developed using the basic principles of structural mechanics considering material deteriorations, and the models were validated with the results of the full-scale testing.
- The results indicate that fire damage does not significantly affect the seismic performance of reinforced precast concrete columns for fire durations up to 60 minutes.

PCI Journal (ISSN 0887-9672) V. 65, No. 6, November–December 2020.
PCI Journal is published bimonthly by the Precast/Prestressed Concrete Institute, 8770 W. Bryn Mawr Ave., Suite 1150, Chicago, IL 60631.

Over the past few decades, precast concrete structural members have been a product of choice in the United States wherever people need to rapidly build homes and industrial facilities.[1] With this popularity, reinforced precast concrete structural members are widely used in structural systems for buildings in seismic zones of both developed and developing countries. Generally, socket base connections are the simplest way to connect reinforced precast concrete columns to foundations, and are mostly used for low-rise buildings, bridge piers, and other light industrial facilities.[2] In such column-to-foundation connections, the bottom of the column is inserted into a reinforced concrete hollow-core body and grouted in place. Reinforced precast concrete columns are prominent load-bearing members in frame buildings that are subjected to seismic loading. Particularly in industrial facilities, lateral forces are resisted through cantilever action of the reinforced precast concrete columns. The majority of European industrial facilities consist of reinforced precast concrete frames, and these structures have demonstrated poor seismic behavior when connections were insufficiently detailed, potentially threatening the life safety of occupants after an earthquake.[3] Reinforced precast concrete structures that were not properly designed and constructed according to the relevant specifications have experienced serious damage, large lateral displacements, and total collapse in previous earthquakes.[3,4]

Most building codes require that reinforced concrete structural members remain standing after a fire event as well as after a design earthquake so that occupants are able to escape from the building and rescue operations can be conducted safely. However, fire damage complicates the assessment of the seismic behavior of structural members depending on the deterioration of the materials, such as concrete and steel reinforcement, which is not generally taken into account during the design stage and is of vital importance for postfire performance assessment. In postfire performance assessment, it should be decided whether to repair, strengthen, or demolish and rebuild the entire structure, taking into account the service and earthquake loads during the remaining service life of the structure. Furthermore, in addition to the need for postfire performance assessment of individual fires, structural fires may also occur because of earthquakes, potentially causing a significant number of casualties. The fires following the 1906 San Francisco, Calif., and 1923 Tokyo, Japan, earthquakes rank as two of the largest urban fires in history. After these two major earthquakes, fires caused about 150,000 deaths and destroyed over 150,000 buildings.[5] Severe earthquakes are typically followed by aftershocks, and therefore structures that have been exposed to fires may be exposed to seismic actions again. The risk of aftershocks following the main shock underscores the obvious need for postfire seismic performance evaluations.[6]

This study focuses on estimating the postfire seismic performance of flexure-dominated reinforced precast concrete columns, which has not been previously investigated. Although the behavior of cast-in-place reinforced concrete columns at elevated temperatures has been extensively investigated under service loads and under service loads combined with uniaxial/biaxial bending after cooling, experimental studies on the postfire seismic behavior of cast-in-place reinforced concrete columns are extremely rare.[7–15] Yaqub and Bailey[16] and Bailey and Yaqub[17] described the results of an experimental study to investigate the seismic performance of shear critical post-heated reinforced concrete columns that had been repaired. In these studies, a uniform temperature exposure was applied and the effects of fire damage on hysteretic response were addressed for fiber-reinforced-polymer (FRP) retrofitting. These studies considered cast-in-place reinforced concrete columns with insufficient shear capacity and focused on retrofitting to enhance the shear capacity of substandard existing buildings.

Bénichou et al.[6] presented the results of a study on the seismic resistance of FRP-strengthened concrete members after fire exposure. Two square and five circular reinforced concrete columns with FRP confinement and fire insulation were exposed to standard fire for four hours. Then, a pushover lateral load was gradually applied. Furthermore, a numerical evaluation was conducted using the structural analysis software SAFIR.[18,19] Because a fire-exposed column specimen without FRP confinement was not available in the study, a simplified approximation using the axial-shear-flexure interaction method was used to estimate the unfired lateral load capacity of one of the columns in numerical calculations. It was reported that the bare column (unconfined and fire exposed for four hours) experienced a 55% reduction in its maximum lateral load capacity due to fire damage, and the maximum drift estimated for this column was 0.03, corresponding to about a 200% increase in deformation capacity compared with a reference specimen that was kept at room temperature.

To the authors' best knowledge, there is no experimental study in the literature that considers the postfire seismic behavior of flexure critical reinforced concrete columns, which are commonly used all over the world. Furthermore, the present study is also unique because it addresses the postfire seismic behavior of reinforced precast concrete columns. The previously mentioned points show that the residual structural capacity of fire-damaged reinforced precast concrete structures subjected to earthquakes is not well known, meaning that many fire-damaged structures could be demolished after a fire when it is not necessary.[20–21] The objective of this paper is to determine the postfire seismic behavior of reinforced precast concrete columns and to use this knowledge to develop safer and more cost-effective postfire structural repair and remediation methods through enhanced postfire performance assessment.

Materials and specimen details

Four reinforced precast concrete columns with 2800 mm (110 in.) height and 300 × 300 mm (12 × 12 in.) cross-sectional dimensions were manufactured. The precast concrete columns were then inserted into reinforced concrete footing sockets. The embedded parts of the columns within the footings were 600 mm (24 in.) long with a gap of 25 mm (1 in.) on all sides. The outer dimensions of the footings were 700 × 700 × 825 mm (27.6 × 27.6 × 32.5 in.). The 25 mm wide gap between the column and the inner walls of the footing was then grouted in place. The surfaces of the embedded parts of the precast concrete columns and inner walls of the footing socket were not subjected to any special treatment (**Fig. 1**). The ready-mixed concrete used in the production of the specimens was provided by a private precast concrete company representing the common practice. **Table 1** gives the properties of the concrete. The concrete contained 78% calcareous aggregates, and 28-day concrete cylinder tests showed a concrete compressive strength of 32.4 MPa (4.7 ksi). The columns were fitted with four 20 mm (0.8 in.) diameter longitudinal steel deformed reinforcing bars placed at the corners with a 50 mm (2 in.) concrete cover from the edge of the specimen to the center of the longitudinal reinforcing bar. These reinforcing bars had a yield strength of 461 MPa (66.9 ksi). Lateral reinforcement with a yield strength of 472 MPa (68.5 ksi) was provided in the form of 10 mm (0.4 in.) diameter ties spaced at 100 mm (4 in.) center-to-center for most of the column height. Along the top 600 mm length of the columns, ties were placed at a spacing of 75 mm (3 in.) center to center. The ratio of the longitudinal and lateral reinforcements of the columns at the core concrete section were calculated according to Eq. (1) and (2), as 2.5% and 0.7%, respectively.

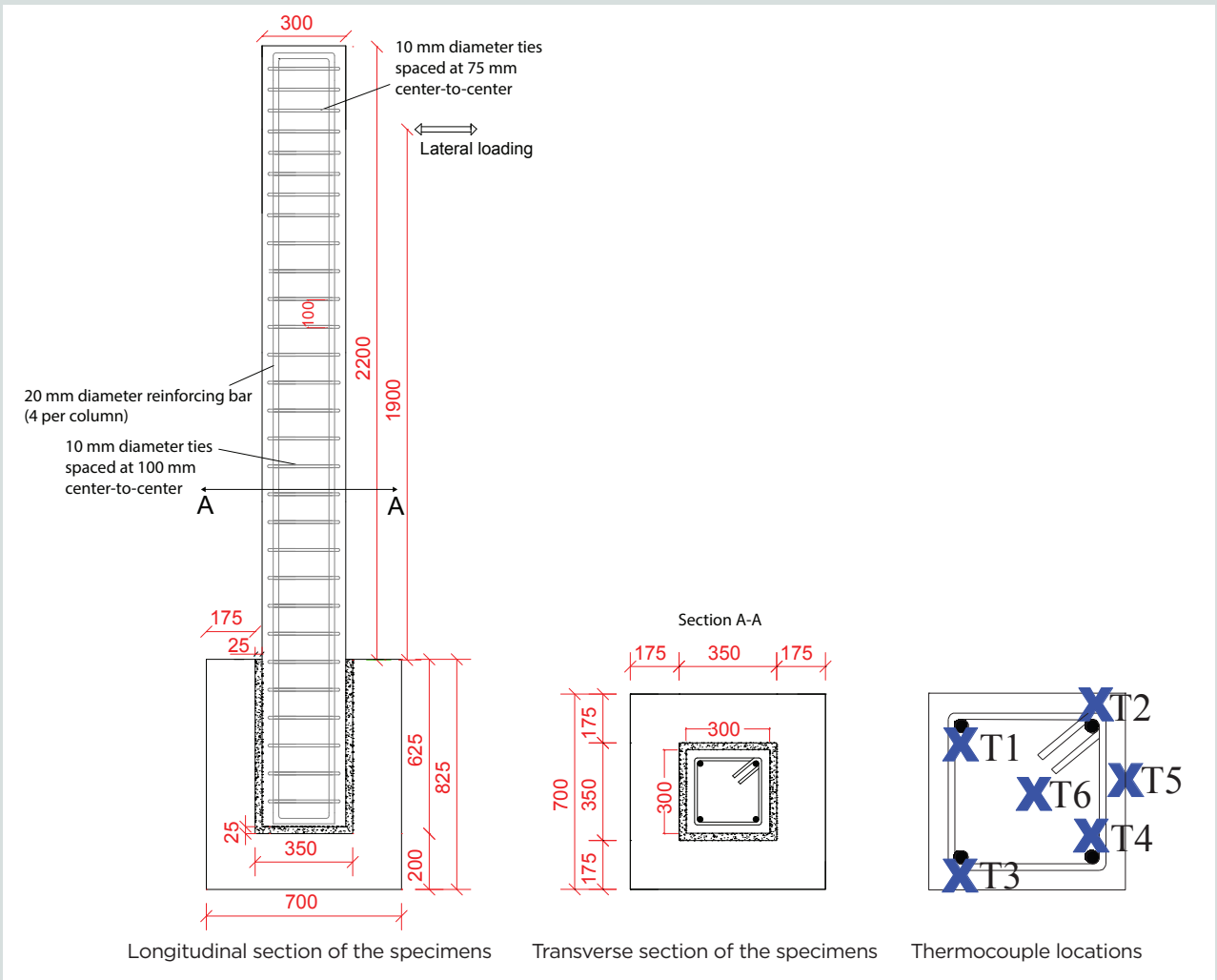

Figure 1. Longitudinal and transverse sections of the specimens and thermocouple locations. Note: All dimensions are in millimeters. 1 mm = 0.0394 in.

$$\rho_l = \frac{A_s}{A_{cc}} \quad (1)$$

$$\rho_t = \frac{A_o}{s} d_c \quad (2)$$

where

ρ_l = ratio of longitudinal steel reinforcement

A_s = area of longitudinal steel reinforcement

A_{cc} = area of concrete core section

ρ_t = ratio of lateral reinforcement

A_o = area of lateral reinforcement

s = spacing of the lateral reinforcement

d_c = concrete core dimension to centerline of the perimeter tie

The seismic design of the specimens was in accordance with the Ministry of Public Works and Settlement's *Specification for the Buildings to be Built in Disaster Areas* (Turkish seismic design code).[22] The designation of the columns is as follows:

- PC-REF is the unheated column.
- PC-30M represents the fire exposure time of 30 minutes.
- PC-60M represents the fire exposure time of 60 minutes.
- PC-90M represents the fire exposure time of 90 minutes.

Socket foundations were overdesigned and insulated against fire. The grout filling the gap between the footing and the column was not insulated and was exposed to fire, like the columns. A commonly used cement-based, nonshrink expand-

Table 1. Mixture proportions and properties of concrete

Material	Quantity
Portland cement (42.5R), kg/m³	300
Sand (0 to 4 mm), kg/m³	920
No. 1 aggregate (5 to 12 mm), kg/m³	507
No. 2 aggregate (12 to 22 mm), kg/m³	490
High-range water-reducing admixture, kg	3.6
Water, kg/m³	124
Slump, mm	200
28-day compressive strength, MPa	32.4
Test day compressive strength, MPa	36.2

Note: 1 mm = 0.0394 in.; 1 kg = 2.205 lb; 1 kg/m³ = 1.69 lb/yd³; 1 MPa = 0.145 ksi.

ing grout was used to fill the gap between the column and the socket foundation. At 28 days, the cube (70 mm [2.75 in.]) compressive strength of the grout was 65 MPa (9.4 ksi) and the flexural strength was 9 MPa (1.3 ksi).

Fire tests

The columns were cured at ambient temperature and humidity for 14 months and then transported to the facility where the fire tests were conducted. The moisture content of the specimens was about 2.5%. The fire furnace was 3.2 × 4.0 m (10.5 × 13.1 ft) in plan and 3 m (9.8 ft) in height (**Fig. A.1**) (for appendix figures, go to https://www.pci.org/2020Nov-Appx-Dem). The furnace consisted of aerated autoclaved concrete walls and slab. The heat was provided by eight gas burners positioned on opposite sides of the furnace. The furnace temperature was set in accordance with the International Organization for Standardization's *Fire Resistance Tests—Elements of Building Construction—Part 1: General Requirements* (ISO 834-1:1999)[23] during the heating stage, which was calculated using Eq. (3).

$$T = 20 + 345\log(8t + 1) \quad (3)$$

where

T = furnace temperature

t = time

After following the fire temperature curve for 30, 60, and 90 minutes, the furnace was switched off and natural air cooling was adopted until the specimens cooled to room temperature (**Fig. 2**). Figure 2 shows that the furnace followed the ISO 834 time-temperature curve, which is similar to the ASTM International fire temperature curve, for each test duration.[24]

The temperatures of concrete and reinforcement were monitored by six K-type NiCr-Ni thermocouples embedded within each specimen during fabrication (Fig. 1). Thermocouples at various locations in the furnace (Fig. A.1) were used to measure the furnace temperature. After 30, 60, and 90 minutes of fire exposure, maximum furnace temperatures of 841°C, 945°C, and 1005°C (1545°F, 1733°F, and 1841°F) were measured, respectively (Fig. 2). In all fire tests, after about 10 minutes of heating, vapor began to come out of the furnace and continued until the end of the test. No spalling sound was detected during the test of column PC-30M, but many irregular hairline cracks appeared on the concrete surfaces of this specimen after heating. A few areas of minor concrete spalling were observed in column PC-60M after 25 minutes of heating. A large total amount of spalling occurred in PC-90M in the form of many small concrete spalls. Because the fire-induced pore pressure increased, spalling was a larger factor for this specimen. **Figure 3** shows the heated columns after cooling. Because of dehydration, light gray formations were observed over the concrete surfaces of PC-30M and PC-60M, whereas the surface of PC-90M was yellowish after heating. During the cooling stage, the temperature continued to rise toward the center of the specimens for up to 5 hours, depending on the duration of the fire exposure, then decreased at a slower rate until the heat balance was achieved. After the first 30 minutes of cooling, furnace temperature decreased to about half of the maximum temperature, then the cooling rate slowed to about 2°C/min (67.6°F/min). The furnace door was kept closed for about 24 hours after cooling started.

Theoretical postfire seismic capacities

The impact of postfire seismic loading on the reinforced precast concrete columns was estimated through combined thermal and structural modeling. At the thermal analysis stage, SAFIR, a finite element analysis software, was used for cross-sectional thermal numerical evaluation over a quarter of the column cross section (**Fig. 4**).[19] The software assumes that heat is distributed in solid structures essentially by conduction, and at the boundary of the structure, heat is exchanged with the environment by convection and radiation. For conduction in concrete, heat exchange is based on a Fourier equation expressed in a Cartesian system of coordinates (Eq. [4]).

$$\frac{\partial}{\partial x}\left[k\frac{\partial T}{\partial x}\right]+\frac{\partial}{\partial y}\left[k\frac{\partial T}{\partial y}\right]+\frac{\partial}{\partial z}\left[k\frac{\partial T}{\partial z}\right]+Q=c\rho\frac{\partial T}{\partial t} \quad (4)$$

where

x = vector of Cartesian coordinates

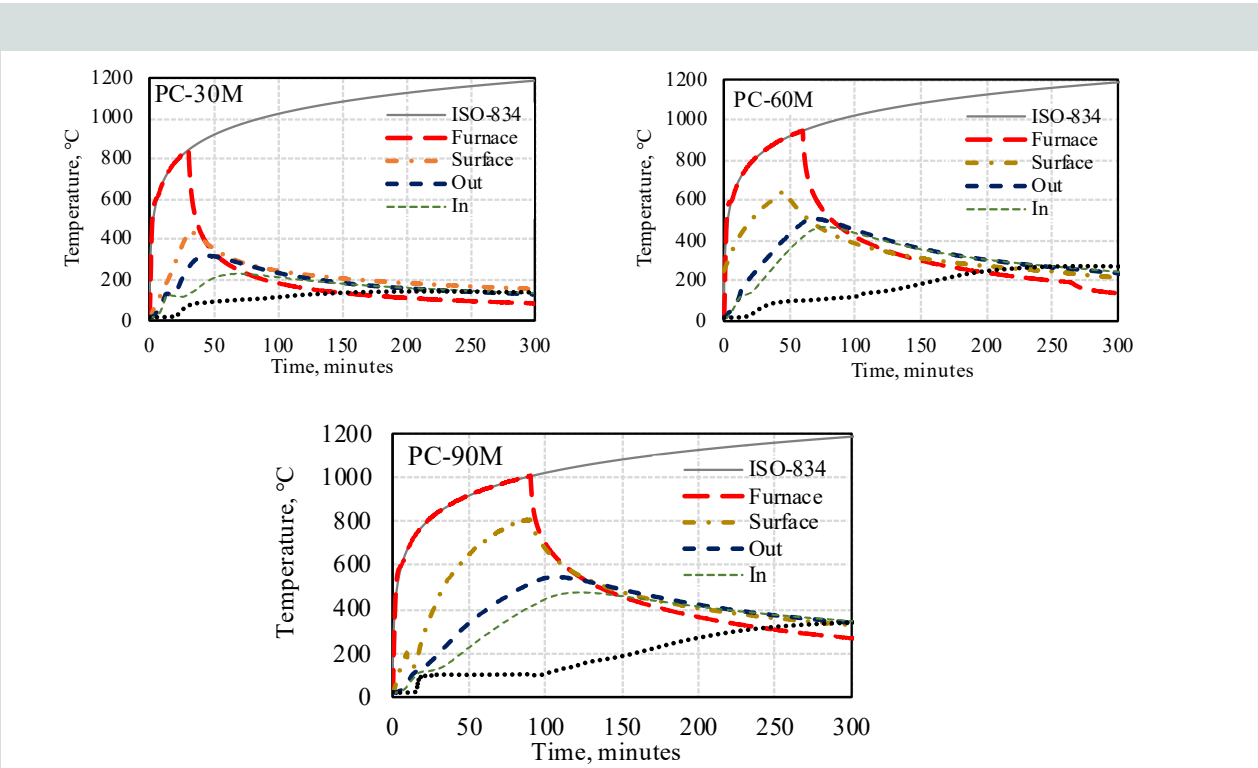

Figure 2. Time-temperature curves in the furnace during the fire tests and after cooling. Note: Surface is obtained from T5, out is obtained from T2 and T3, in is obtained from T1 and T4, and center is obtained from T6. 1°F = 1°C × 1.8 + 32.

k = thermal conductivity

y = vector of Cartesian coordinates

z = vector of Cartesian coordinates

Q = constant for internal generation of heat

c = specific heat

ρ = specific mass

For convection and radiation acting over the structure's boundaries with the surrounding environment, heat exchange is evaluated using Eq. (5) and (6).

$$h_c = h_{cc}(T_g - T_s) \quad (5)$$

where

h_c = convective heat flux between gas and solid

h_{cc} = coefficient of convection

T_g = temperature of the gas

T_s = temperature at the surface of the solid

$$h_r = \sigma \varepsilon T_s^4 \quad (6)$$

where

h_r = radiative heat flux emitted by a solid

σ = Stefan-Boltzmann constant

ε = emissivity of the solid

The software uses an iterative process that evaluates the temperatures at multiple time steps until thermal equilibrium is established. In thermal modeling with SAFIR, column cross sections were defined by 144 nodes and 121 solid elements, and then experimentally obtained time-temperature relationships including the cooling phase were defined for the fire-exposed edges of the section. Calcareous concrete and steel material properties were assigned to the corresponding elements of the cross section as given by the European Committee for Standardization's *Eurocode 2: Design of Concrete Structures—Part 1-2: General Rules—Structural Fire Design* (Eurocode 2).[25] Experimentally measured thermocouple readings (Fig. 2) were used to verify the findings of SAFIR (Fig. 4), which were found to be satisfactory.

Thermal analysis results were then implemented into structural modeling to predict the postfire lateral load-displacement response of the columns. **Figure 5** shows the step-by-step structural analysis procedure. The theoretical seismic responses of the fired and unfired columns were calculated considering the moment-curvature relationships of the columns at the

Figure 3. Postcooling appearance of the columns.

critical sections based on fiber analysis approach and plastic hinge concept. The effect of axial loading was considered in the fiber analysis. In the fiber analysis, reinforced concrete column cross sections were divided into 36 finite elements each having dimensions of 50 × 50 mm (2 × 2 in.) (**Fig. 6** and step 1 of Fig. 5). Average temperatures for each element attained during the whole course of heating and cooling, were taken from the thermal analyses conducted by SAFIR, which were verified by thermocouple readings obtained from the fire tests (Fig. 2 and step 2 of Fig. 5). The average temperatures for the elements were then interpolated based on the temperatures calculated along both the diagonal section and symmetry axis of the section (Fig. 6), similar to the method of Mostafaei et al.[26] Using the calculated temperatures, the residual stress-strain relationship for each of the finite elements was determined using Eq. (7) and (8), as recommended by Chang et al.[27] (step 3 of Fig. 5).

$$\frac{f_{cT}^{'}}{f_{c}^{'}} = 1.01 - 0.00055T \text{ for } 20°C < T \le 200°C \ (68°F < T \le 392°F)$$
$$= 1.15 - 0.00125T \text{ for } 200°C < T \le 800°C \ (392°F < T \le 1472°F) \quad (7)$$

where

$f_{cT}^{'}$ = residual compressive strength of concrete after exposure to temperature T

$f_{c}^{'}$ = concrete compressive strength at ambient temperature

$\frac{\varepsilon_{oT}}{\varepsilon_{o}} = 1$ for 20°C < T ≤ 200°C (68°F < T ≤ 392°F)

$$= \left\{\left(-0.1f_{c}^{'} + 7.7\right)\left[\frac{\exp(-5.8 + 0.01T)}{1 + \exp(-5.8 + 0.01T)}\right] - 0.0219\right\} \quad (8)$$

for 200°C < T ≤ 800°C (392°F < T ≤ 1472°F)

where

ε_{oT} = residual peak compressive strain of concrete after exposure to temperature T

ε_{o} = compressive peak strain at ambient temperature

To verify the actual compressive strength of each finite element, concrete core samples were taken from undamaged regions of the reinforced concrete columns after the seismic tests were conducted. A total of two single-core samples with a diameter of 100 mm (4 in.) and a height of 300 mm (12 in.) were taken along the whole width and depth of each column, and each sample was then divided into six parts, each having a diameter of 100 mm and height of 50 mm (2 in.). These samples were tested under uniaxial compression loads to verify the compressive strength of each fire-exposed concrete element shown in Fig. 6. Because measuring compressive strains over these core samples would not be realistic due to the unconventional dimensions of the samples, 150 × 300 mm (6 × 12 in.) standard cylinders were subjected to the same fire tests as the reinforced concrete columns. The stress-strain behavior of these cylinder specimens was obtained under uniaxial compression loads. **Figure A.2** shows the variations of stress-strain relationships obtained from standard cylinder specimens after fire tests and variations of average compressive strengths of the cores and the cylinder samples. A stan-

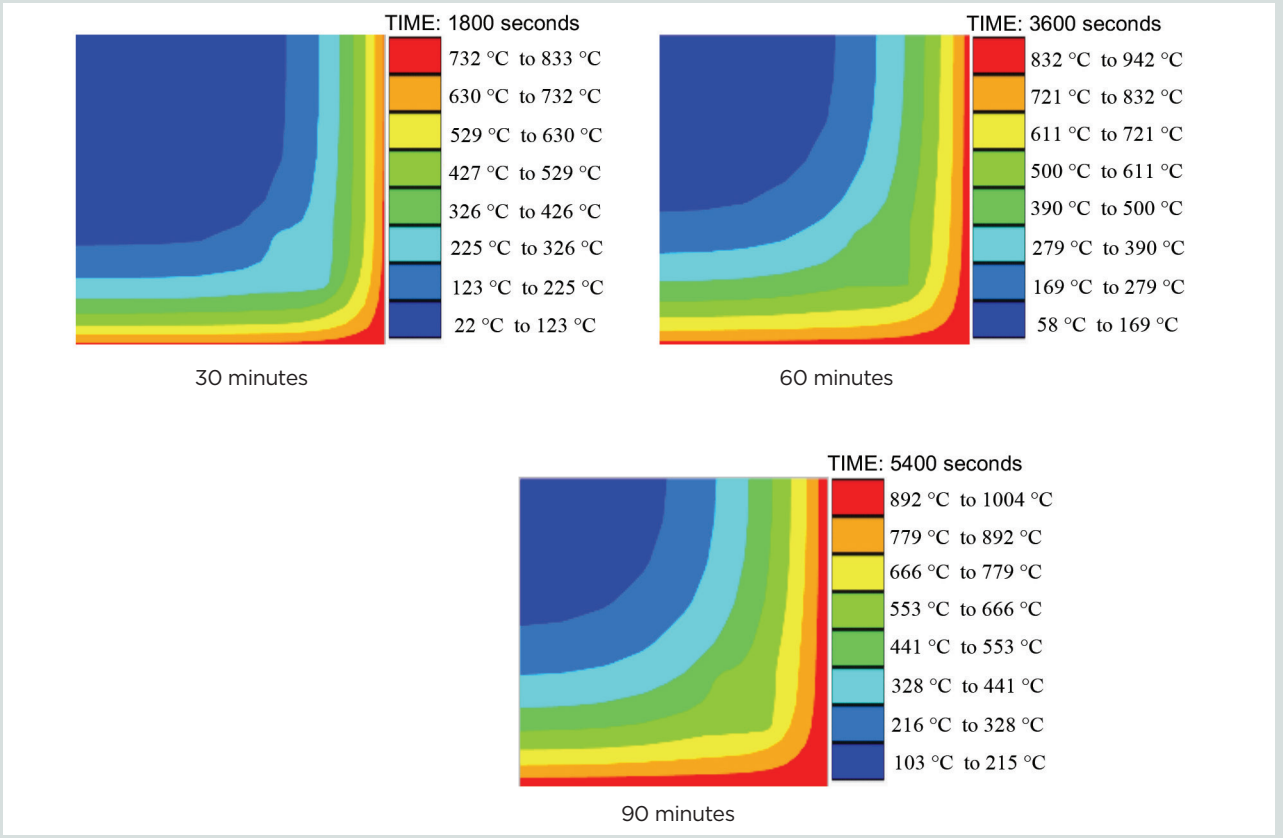

Figure 4. Temperature distributions in fire tests obtained from the thermal analysis software SAFIR for 30, 60, and 90 minutes. Note: 1°F = 1°C × 1.8 + 32.

dard naming convention was used for the specimens shown in Fig. A.2. For example, REF represents an unheated specimen and C1-30M-1 represents the first cylinder specimen of the sample series exposed to fire for 30 minutes (30M).

Experimentally obtained compressive strengths and strains were found to be in reasonable agreement with the analytically estimated model findings from Eq. (7) and (8). Core compressive strengths were converted to standard cylinder strengths with a conversion factor calculated based on the ratio of cylinder to core compressive strengths obtained from the unheated specimens (that is, 36.2/30.8 in Fig. A.2). Therefore, model predictions obtained using Eq. (7) and (8) were used in the structural analysis for defining unconfined concrete properties after fire exposure, which were validated by the core strengths (converted to cylinder strengths) and heated cylinder peak compressive strains given in Fig. A.2. Figure A.2 also gives the stress-strain relationships used in the fiber analysis for the unheated (unfired) elements and elements heated (fired) for 90 minutes.

The model developed by Mander et al.[28] was used to estimate confined concrete properties after fire exposure, and actual uniaxial tensile test results of reinforcement were used in the analysis (step 4 of Fig. 5). To obtain the mechanical properties of the reinforcement, 300 × 300 × 500 mm (12 × 12 × 18 in.) reinforced concrete specimens, which had the same reinforcing as the full-scale reinforced concrete columns, were cast using the same concrete batch. These specimens were then subjected to the same fire exposure as the full-scale columns. The reinforcing bars were removed from the concrete after cooling and subjected to uniaxial tension tests.

Table 2 presents the mechanical properties of the longitudinal (20 mm [0.8 in.]) diameter) and transverse (10 mm [0.4 in.] diameter) reinforcing bars at ambient temperature and after cooling. The table gives properties based on the average of four samples and shows that the differences of the tensile test results between the fired and unfired specimens were almost negligible (less than 5%). There is no remarkable difference between the mechanical properties of the unfired reinforcing bars and the reinforcing bars exposed to fire for 90 minutes (the most severe fire) because the measured maximum temperatures along the reinforcement did not exceed 510°C (950°F) during the fire tests, including the cooling phase (Fig. 2). The residual properties of the reinforcing bars are thus estimated to be almost recovered for all fire exposure durations (30, 60, and 90 minutes) as experimentally shown in this study (Table 2) and also reported in the literature for these temperature ranges.[29] For the sake of conservatism, the small difference between the residual properties of the fired and unfired reinforcement was also considered in the fiber

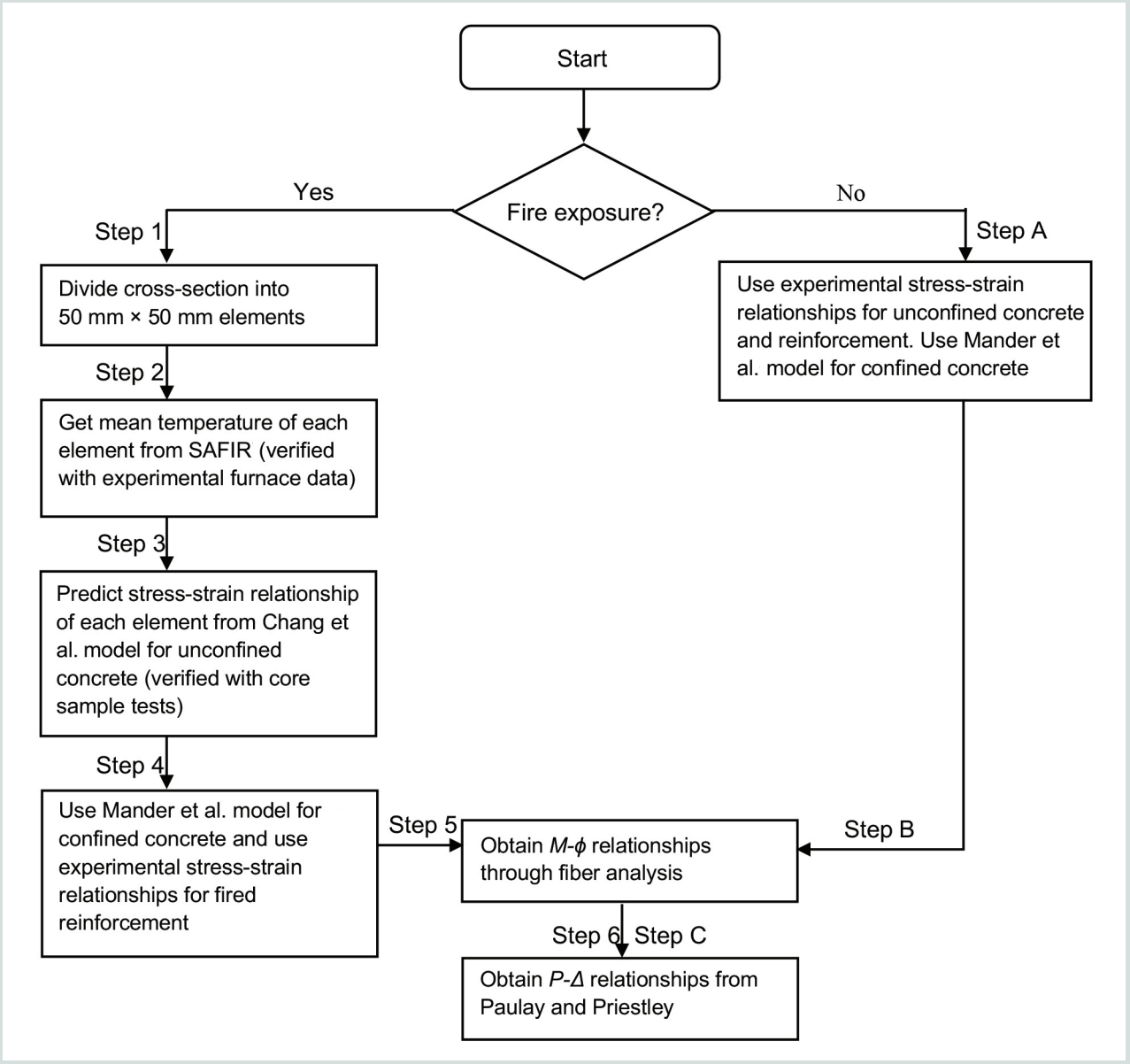

Figure 5. Calculation procedure for the prediction of postfire *P-Δ* relationships of the columns. Note: *M* = moment; *P* = lateral load; *Δ* = lateral displacement; *ϕ* = curvature. 1 mm = 0.0394 in.

analysis, and the test results for specimens exposed to fire for 90 minutes were used in modeling all fire-exposed reinforcement (step 4 of Fig. 5). For the fiber analysis, steel reinforcing bars were assumed to behave in an elastoplastic manner with strain hardening. For the unfired columns, the actual stress-strain relationships obtained from unheated cylinder specimens (Fig. A.2) were used to define the unconfined concrete properties, whereas the Mander et al.[28] model was used for confined concrete (step A in Fig. 5 step A). Experimentally obtained mechanical properties were used for the reinforcement (Table 2).

Once the residual mechanical properties of the concrete and reinforcement were determined, monotonic moment-curvature relationships for the columns were obtained at the critical sections of each reinforced concrete column through a fiber analysis approach using commercial software[30] (steps 5 and B of Fig. 5). The moment-curvature relationships were later used to predict the load-displacement relationships (steps 6 and C of Fig. 5). **Figure A.3** shows the theoretically obtained moment-curvature relationships for the columns PC-REF and PC-90M. **Table 3** gives the strains computed for unconfined concrete (extreme concrete compression fiber on the column surface) ε_c, confined concrete (extreme concrete compression fiber on core) ε_{cc}, and longitudinal reinforcing bars in tension ε_s corresponding to specific points on the moment-curvature relationships (Fig. A.3) (that is, for points corresponding to yielding [A and C] and ultimate [B and D] where the analysis stopped). After obtaining the moment-curvature relationships, the total top displacements

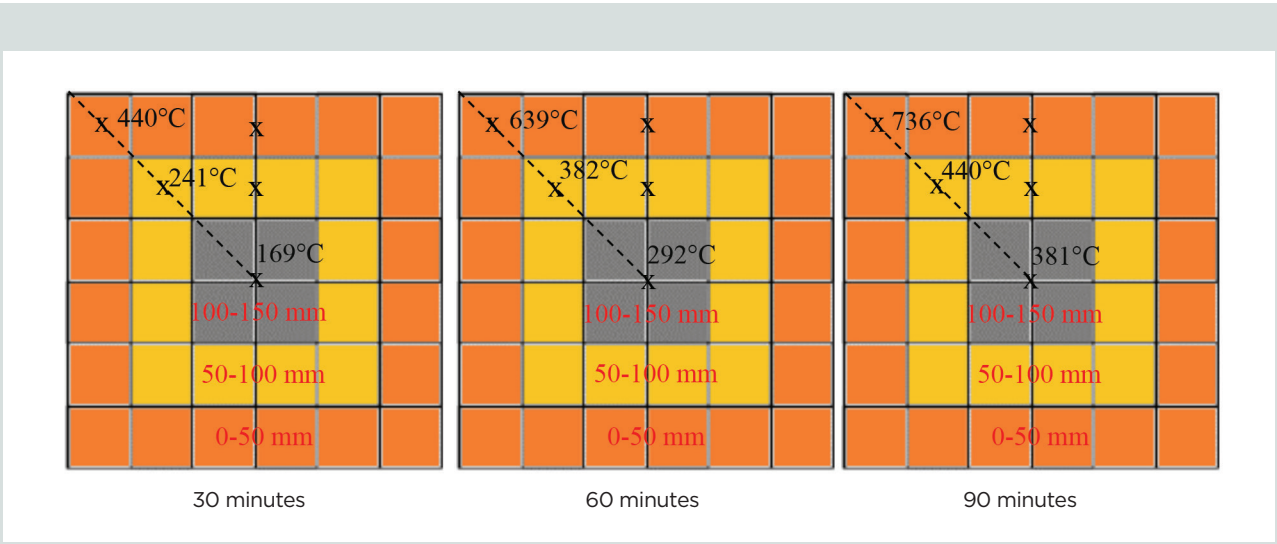

Figure 6. Maximum temperatures including cooling stages after 30, 60, and 90 minutes. Note: 1 mm = 0.0394 in.; 1°F = 1°C × 1.8 + 32.

of the columns were estimated considering the elastic and inelastic deformations using the approximation defined by Paulay and Priestley[31] for prismatic reinforced concrete cantilever columns (steps 6 and C in Fig. 5). The curvature distribution at yield was determined by linear approximation and can be estimated using Eq. (9).

$$\Delta_y = \phi_y l^2/3 \quad (9)$$

where

Δ_y = yield displacement

ϕ_y = yield curvature

l = shear span of the reinforced concrete column

Assuming that the plastic rotations are concentrated at mid-height of the plastic hinge length l_p, the plastic displacement Δ_p at the cantilever tip is calculated using Eq. (10) to (12).

$$l_p = h/2 \quad (10)$$

$$\theta_p = \phi_p l_p \quad (11)$$

$$\Delta_p = \theta_p(1 - 0.5l_p) \quad (12)$$

where

h = depth of the cross section

θ_p = plastic rotation along the equivalent plastic hinge length

ϕ_p = plastic curvature

For the sake of simplicity, the Turkish seismic design code[22] was used to define the plastic hinge length as half the depth of the cross section. The theoretically obtained load-displacement relationships were later compared with the experimental behavior, which is discussed in the following section.

Seismic tests

Seismic performance at different seismic displacement demands of the precast concrete cantilever columns con-

Table 2. Mechanical characteristics of reinforcing bars

Reinforcing bar diameter, mm	Fire exposure, minutes	f_y, MPa	ε_y	f_{max}, MPa	ε_{max}	f_u, MPa	ε_u
20	n/a	472	0.0023	569	0.0965	525	0.15
10	n/a	483	0.0025	557	0.0998	525	0.10
20	90	442	0.0024	549	0.0992	516	0.16
10	90	457	0.0024	552	0.0992	522	0.11

Note: f_{max} = maximum tensile stress; f_u = ultimate tensile stress; f_y = yield stress; n/a= not applicable; ε_{max} = maximum tensile strain; ε_u = ultimate tensile strain; ε_y = yield strain. 1 mm = 0.0394 in.; 1 MPa = 0.145 ksi.

Table 3. Theoretically obtained strains

	PC-REF		PC-90M	
	Point A	Point B	Point C	Point D
Compressive strain of unconfined concrete ε_c	0.0011	0.006	0.0018	0.007
Compressive strain of confined concrete ε_{cc}	0.0007	0.020*	0.0014	0.020*
Tensile strain of longitudinal steel reinforcement ε_s	0.0024†	0.083	0.0024†	0.072

*Crushing of core concrete
†Yielding of reinforcing bar

sidered in this study is expected to be higher with respect to that of cast-in-place columns because of higher flexibility due to higher interstory height observed in industrial building columns and the relatively low flexibility of the supports compared with cast-in-place columns. Because this is the first study considering the postfire seismic behavior of reinforced precast concrete columns, there is an obvious need to better understand hysteretic response to predict seismic performance at different seismic displacement demands for a comprehensive postfire structural performance estimation.

It is important to develop hysteretic models capable of representing all important phenomena related to the deterioration observed in experimental studies. These models will help evaluate the postfire capacity of structures. Therefore, to determine the seismic performance, after exposure to the standard heating, all columns were transported to a laboratory for seismic testing. Seismic tests were conducted under constant axial loads with an axial force level of 315 kN (70.8 kip) and uniaxial lateral load reversals. In Europe, the common practice in precast concrete industrial buildings is to keep the axial load ratio n between 0.05 and 0.20.[32] There-

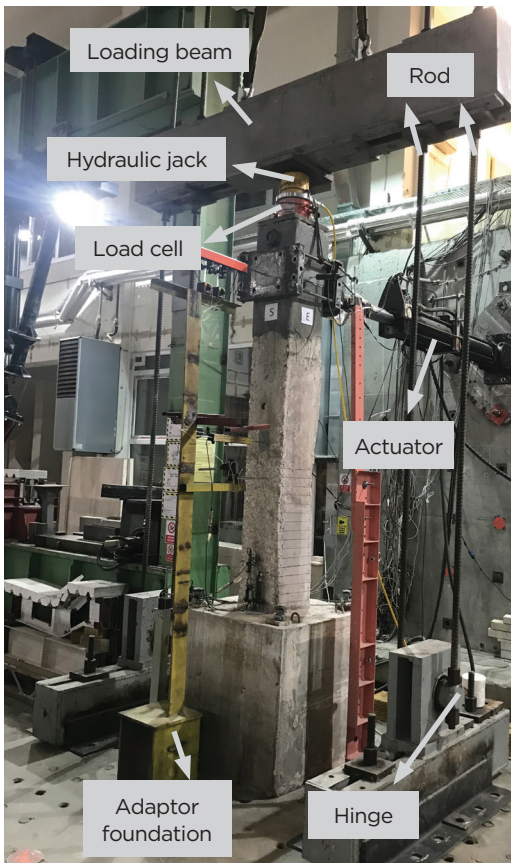

Seismic test setup

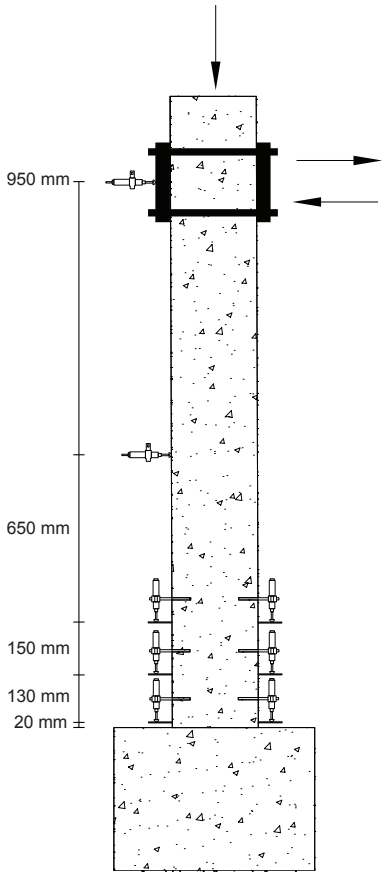

Arrangement of linear variable differential transformers

Figure 7. Seismic test setup and arrangement of linear variable displacement transducers. Note: 1 mm = 0.0394 in.

fore, to reflect the actual axial loads in practice, the axial load in the present study corresponded to 10% of the axial load-bearing capacity, which was calculated using Eq. (13) and (14).

$$n = N/N_0 \quad (13)$$

where

N = applied axial load

N_0 = axial load-bearing capacity of the column considering only the contribution of the concrete

$$N_0 = f_c' A_g \quad (14)$$

where

A_g = gross cross-sectional area of the column

Seismic tests were conducted 75 days after the fire tests, corresponding to the approximate date when structural performance assessment procedures, including the residual structural analysis, are completed. **Figure 7** shows the seismic test setup. All columns were fixed to a strong floor with four 32 mm (1.3 in.) diameter high-strength steel bolts. A hydraulic jack was used between the top of the columns and the steel frame to apply axial loads, and the load cell was inserted between the jack and the loading beam to measure the applied axial loads. Axial loads were applied to the column by a pinned connection from the supported steel frame, which was fixed at the base to the adaptor foundation by steel rods before application of lateral loads simulating seismic loading. Cyclic lateral loads were applied at the top of each specimen at 1900 mm (75 in.) height from the column base by a hydraulic actuator with a capacity of ±250 kN (56 kip) and ±300 mm (12 in.) connected to a strong reaction wall. To monitor the lateral and longitudinal displacements as well as rotations, numerous linear variable displacement transducers were installed at various locations along the height of the columns (Fig. 7). The American Concrete Institute's *Guide for Testing Reinforced Concrete Structural Elements under Slowly Applied Simulated Seismic Loads* (ACI 374.2R)[33] lateral loading protocol was used in the seismic tests (**Fig. A.4**). Target drift ratios, calculated as the ratio of the lateral displacement at the top of the specimen to the specimen height, were ±0.1%, ±0.25%, ±0.5%, ±1%, ±2%, ±3%, ±4%, ±5%, ±6%, ±7%, and ±8% in the pushing and pulling directions, corresponding to top displacements of ±1.9 mm (0.075 in.), ±4.75 mm (0.19 in.), ±9.5 mm (0.37 in.), ±19 mm (0.75 in.), ±38 mm (1.50 in.), ±57 mm (2.24 in), ±76 mm (3.0 in.), ±95 mm (3.74 in.), ±114 mm (4.49 in.), ±133 mm (5.24 in.) and ±152 mm (5.98 in.), respectively. All displacement cycles were repeated twice, as recommended by ACI 374.2R.

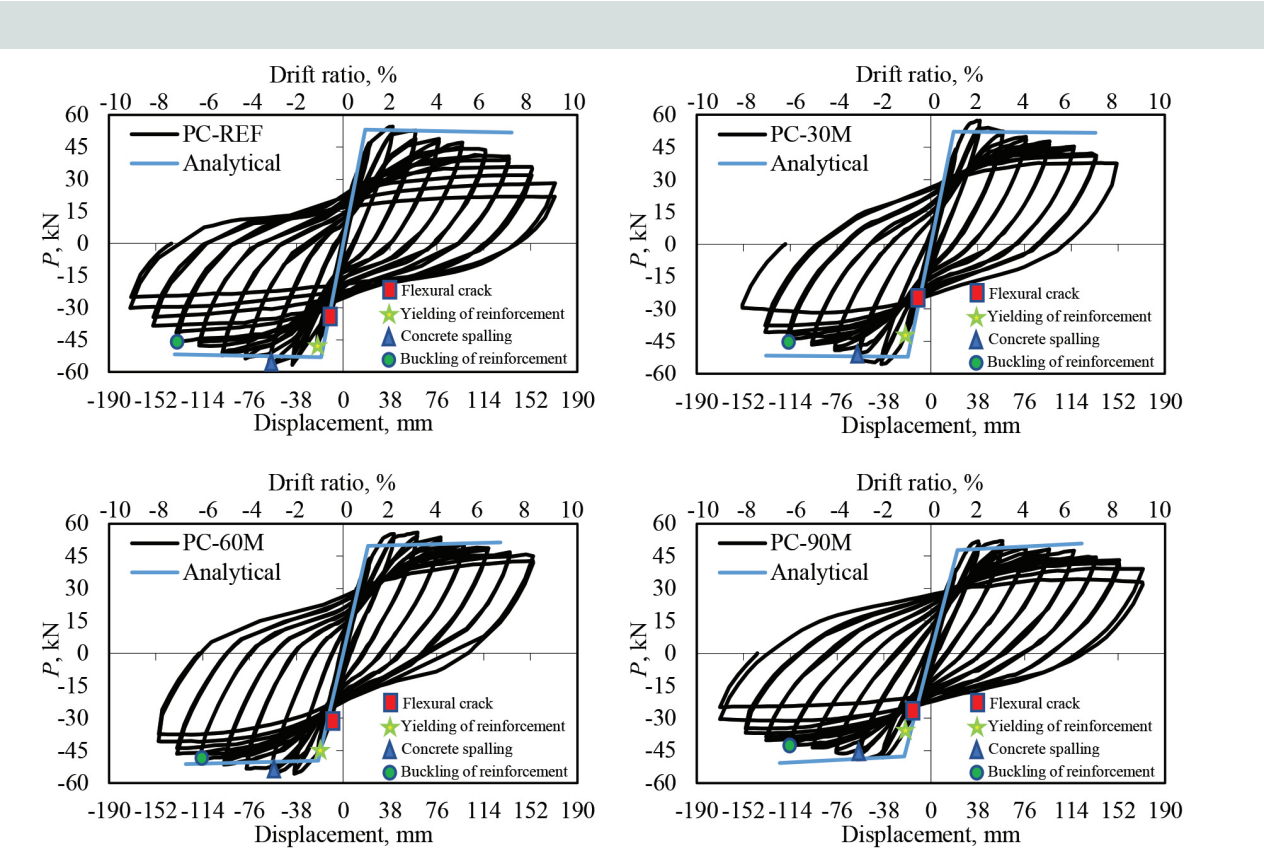

Figure 8. Load-displacement curves of the columns. Note: P = lateral load. 1 mm = 0.0394 in.; 1 kN = 0.225 kip.

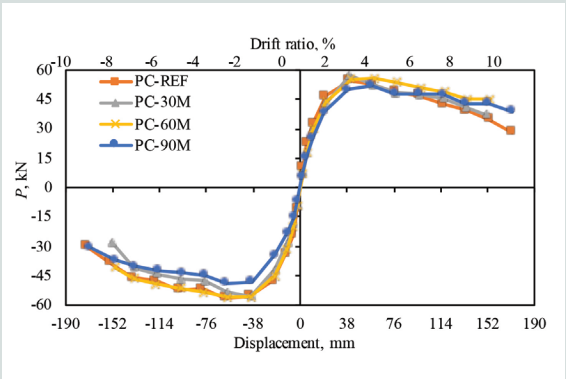

Figure 9. Envelope curves of the columns. Note: P = lateral load. 1 mm = 0.0394 in.; 1 kN = 0.225 kip.

Figures 8 and **9** show, respectively, the lateral-load-displacement hysteretic curves and their envelopes obtained for the tested columns, where P denotes applied lateral load. In the figures, the negative drift ratios correspond to the pushing direction and the positive drift ratios are the pulling direction values. The analytical modeling results given in Fig. 8 accurately predict the lateral-load-displacement behavior of reinforced precast concrete columns. In analytical evaluation, all of the specimens failed with the crushing of the confined concrete because buckling was not included in the fiber analysis. In the experimentally obtained load-displacement curves, failure was caused by the buckling of the longitudinal bars at larger drifts (around 6% drift ratio). The analytical findings of this study show that when the residual properties after fire, such as stress-strain behavior of concrete and reinforcement, are realistically taken into account, the basic principles of structural mechanics are also applicable to postfire seismic performance assessment.

All tested columns reached their theoretical capacities, indicating that the inelastic response of the columns was ultimately dominated by flexure, resulting in ductile behavior (Fig. 8). Peak lateral loads were observed at about 2% drift ratio for the columns PC-REF and PC-30M, whereas columns PC-60M and PC-90M reached their lateral load capacities at about 3% drift ratio.

Figures A.5 and **A.6** show damage to the potential plastic hinge region of the columns after reaching their lateral load capacities at around 2% drift ratio and at the end of the tests, respectively. The columns exhibited a stable deterioration response up to a drift ratio of about 6%, where buckling of the longitudinal reinforcing bars led to subsequent failure and the strength of the columns decreased following strength degradation. Mean values of pulling and pushing direction peak loads (**Table 4**) show that for PC-30M and PC-60M, lateral load capacities were not significantly affected by fire exposure, compared with an approximately 10% reduction in ultimate lateral load for PC-90M. This can be explained by the greater loss in compressive strength of this specimen, leading to lower bending moment capacity and thereby lower lateral load capacity than the other specimens. However, the reductions in lateral load capacities were less than the reductions in the compressive strengths. This can be explained by the low axial loads (315 kN [70.8 kip]) applied during the seismic tests (which is typical for this kind of reinforced precast concrete column in practice, as previously explained), which minimized the impact of compressive strength on the behavior, as shown in the axial-load-moment interaction diagrams (**Fig. A.7**). Theoretically obtained lateral load capacities are in reasonable agreement (less than 7% error) with experimental peak lateral loads (Table 4).

The displacement ductility factor μ_Δ, which is the ratio of the ultimate displacement Δ_u to the yield displacement Δ_y, was calculated for each column to compare the column performance in terms of sustained ductility (**Fig. 10**). Ultimate displacement is defined as the point on the post-peak branch of the average lateral-load-displacement envelope curve (absolute average of pushing and pulling directions) where the lateral load is 80% of the maximum lateral load ($P = 0.8P_{max}$), as recommended by previous researchers.[34–37] Yield displacement is also obtained from the average lateral-load-displacement envelope curve as the displacement corresponding to the maximum lateral load P_{max} plotted on a straight line between the origin and the point at 75% of the peak load on the ascending portion of the envelope curve ($P = 0.75P_{max}$), as recommended by previous researchers.[31] The ductility of the columns was not found to be affected by fire exposure of up to 60 minutes, whereas column PC-90M

Table 4. Lateral load capacities and ductility parameters of the columns

	PC-REF	PC-30M	PC-60M	PC-90M
Experimentally obtained maximum lateral load P_{max}, kN	55.0	56.5	55.9	50.5
Theoretically obtained maximum lateral load P_{max}, kN	55.2	53.7	51.9	51.0
Lateral yield displacement Δ_y, mm	22.2	26.4	25.3	29.8
Lateral ultimate displacement Δ_u, mm	124.9	112.3	142.4	147.1
Ductility factor μ_Δ	5.6	4.3	5.6	4.9

Note: 1 mm = 0.0394 in.; 1 kN = 0.225 kip.

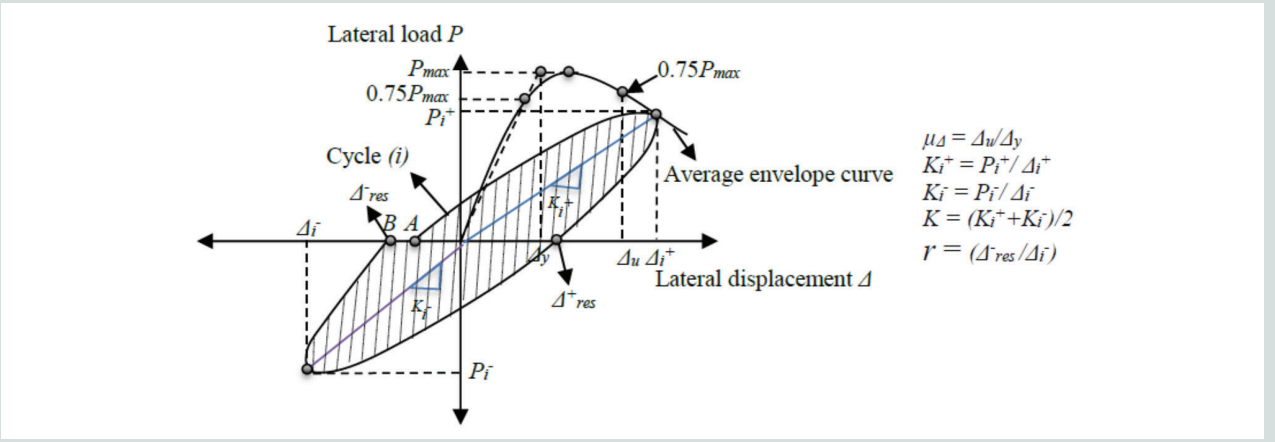

Figure 10. Definition of ductility parameters. Note: i = cycle number; K = secant stiffness; K_i = secant stiffness at cycle i; P_i = lateral load at cycle i; P_{max} = maximum lateral load; r = residual displacement; Δ_i = lateral displacement at cycle i; Δ_{res} = residual lateral plastic displacement when the lateral load is zero; Δ_u = lateral ultimate displacement; Δ_y = lateral yield displacement; μ_Δ = ductility factor.

exhibited about 13% ductility reduction with respect to the reference column (Table 4).

In column PC-30M, local defects in the concrete cover close to the plastic hinge region were observed after the fire tests. Figure 3 shows that these fire-induced vertical cracks (indicated as vertical black lines) advanced remarkably at about 0.5% drift ratio (9.5 mm [0.37 in.] top displacement). This defect caused premature spalling of the concrete cover for this specimen, which resulted in relatively high yield displacement (lower stiffness) and low ultimate displacement and ductility factor. Even though fire exposure increased both the yield and the ultimate displacements of the fire-exposed specimens (except for PC-30M due to the aforementioned phenomenon), the main deficiency related to the fire damage occurred in the ductility ratio of column PC-90M because the increase in yield displacement was greater than the increase in ultimate displacement. As a general consequence of the findings previously mentioned, it is noteworthy that fire exposure enabled larger displacements at a cost of reduced lateral strength. Stiffness degradation of column PC-90M due to fire exposure arose from higher yield and ultimate displacements with respect to the unheated column. Nevertheless, previous researchers reported that displacement ductility factors higher than 3.5 correspond to a fully ductile response that can reasonably be achieved at carefully identified and detailed inelastic regions.[31] When this value (3.5) is compared with the values given in Table 4, the postfire ductility of all columns appears to be satisfactory in terms of structural response.

Loss of stiffness due to fire exposure is a key parameter to be considered in the postfire performance assessment of reinforced concrete members. To evaluate stiffness degradation after a fire, secant stiffness K values of the columns were determined by dividing the maximum lateral load of each cycle by the displacement at the peak of each load cycle considering the mean value of the pushing and pulling directions (Fig. 10).

Figure 11 compares the variation of secant stiffness with the horizontal displacement and shows that the initial stiffness values for the fire-exposed columns were substantially lower than for PC-REF. The reductions in initial stiffness were about 7%, 20%, and 33% for columns PC-30M, PC-60M, and PC-90M, respectively, compared with column PC-REF. However, the rate of postcracking stiffness degradation was more pronounced in PC-REF compared with the heated columns. New cracks initiated after imposing cyclic loading for the unheated specimen (PC-REF), while fire-induced existing cracks advanced for the fire-exposed columns. Therefore, a slower rate of stiffness degradation was observed in the fire-exposed specimens than in the reference specimen, which is beneficial for reinforced precast concrete columns subjected to seismic actions because brittle failure related to sudden loss of stiffness is eliminated. Fire exposure had a greater effect on the residual stiffness at smaller drift ratios, whereas the stiffness of the columns was similar after about 2% drift ratio (around yielding). This is because the structural response is governed by concrete residual properties up to yielding, whereas after yielding, the reinforcement characteristics that are restored after cooling are more dominant.

The area enclosed by the first hysteretic loop of each target displacement is defined as the energy dissipated by the columns, which represents the ability to consume seismic energy through plastic deformations. Figure 11 plots the cumulative hysteretic energy dissipation capacities of the columns, which are the summations of these areas (Fig. 10), at increasing drift ratios. The figure clearly indicates that the lowest energy was dissipated by PC-90M due to the relatively low lateral load capacity, while it was similar among the other specimens. The energy dissipation capacities of the columns were similar up to 2% drift ratio (around yielding), whereas the rate of increase in energy dissipation capacity was found to be greater for the columns other than PC-90M after yielding. This is because after yielding, most of the energy was consumed by the

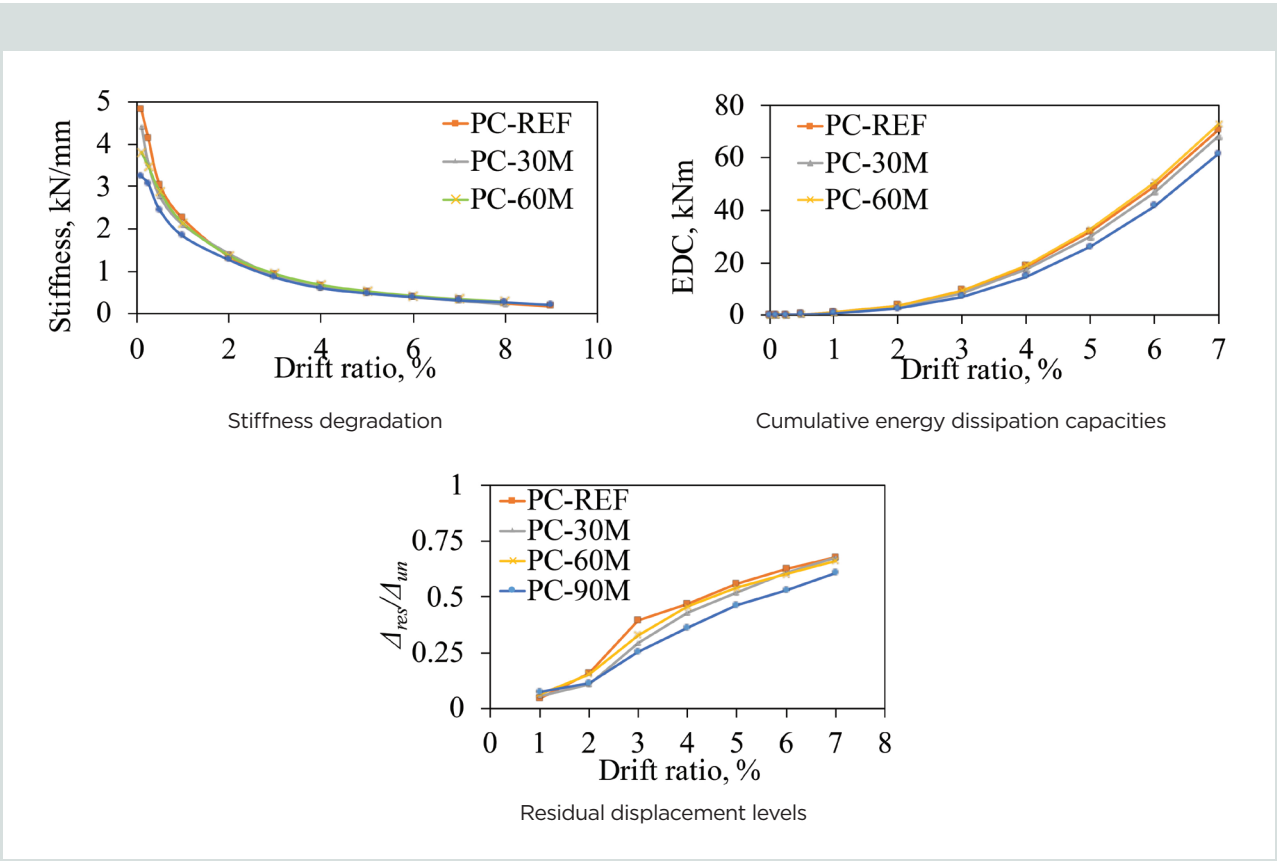

Figure 11. Stiffness degradation, cumulative energy dissipation capacities, and residual displacement levels for the columns. Note: EDC = energy dissipation capacity; Δ_{res} = residual lateral plastic displacement when the lateral load is zero; Δ_{un} = specified peak displacement for each drift ratio. 1 kN-m = 0.74 kip-ft; 1 kN/mm = 5.71 kip/in.

inelastic deformation of the columns, including the formation of new cracks and the yielding of reinforcing bars. The energy dissipation capacity was about 15% less in PC-90M at 7% drift compared with PC-REF, while the difference between the other specimens was less than 5%. No appreciable pinching was observed in the load-displacement curves of the columns, highlighting acceptable performance in terms of energy dissipation.

Residual displacement is one of the most important parameters for measuring postearthquake functionality and the feasibility of repairing fire-damaged structures. The residual plastic displacement ratios *r* of the columns are obtained by dividing the residual lateral plastic displacements after unloading when the applied lateral load is zero Δ_{res} by the specified peak displacement for each drift ratio Δ_{un} in the pushing direction (Fig. 10). Figure 11 gives the *r* values with increasing drifts and shows that after flexural yielding, the *r* values are lowest for PC-90M, whereas they are similar for the other columns, demonstrating greater permanent flexural damage associated with yielding of the reinforcing bars in PC-90M.[38] The lower residual displacements for PC-90M can be attributed to the reduced postyield stiffness induced by fire exposure, and the impact of bond deterioration on this issue can be limited. The limited bond deterioration can be validated considering the good agreement between the theoretical and experimental test results (Fig. 8) as well as the minor differences in residual displacements for all specimens (Fig. 11). At 7% drift, the residual plastic displacement ratio was about 0.65 for columns PC-REF, PC-30M, and PC-60M and about 0.6 for PC-90M, corresponding to an approximately 10% reduction in plastic deformations for PC-90M with respect to the other specimens. The relatively low residual deformations observed in PC-90M are considered a positive property under seismic loads.

Figure A.8 presents the base moment-average curvature relationships for the columns. In the figure, the negative values correspond to the pushing direction and the positive values correspond to the pulling direction. The base moment was calculated by multiplying the measured lateral load by the shear span of 1900 mm (75 in.) extending between the acting point of the lateral load and the column–foundation interface, where the contribution of the axial load was also taken into account. The curvature distributions of the columns were measured using displacement transducers attached at the potential plastic hinge region over heights of 0 to 20 mm (0 to 0.8 in.), 20 to 150 mm (0.8 to 6 in.), and 150 to 300 mm (6 to 12 in.) above the column–foundation interface (Fig. 7). Because the low axial forces and closely spaced stirrups provided effective confinement, large plastic rotations in the plastic hinge regions were observed for all specimens. The curvature was concentrated mainly over a height of approximately 0 to

150 mm for PC-REF and PC-30M, which is the half depth *h*/2 of the column cross section (Fig. A.8). This height was between 0 and 300 mm for PC-60M and PC-90M, corresponding to full depth *h* of the column dimensions in the loading direction. This behavior indicates that flexural damage was distributed over a larger plastic hinge length for PC-60M and PC-90M than for PC-REF and PC-30M. This is attributed to the considerable loss of concrete compressive strength with an increase in fire duration, which resulted in a loss of axial load capacity and thereby an increase in axial load ratio (applied axial load divided by axial load capacity). Axial load ratio has an important influence on the plastic hinge length of reinforced concrete columns, and plastic hinge length elongates with an increase in the axial load ratio.[39] Furthermore, the formation of cracks was observed during the cyclic loading to be distributed over a larger hinging zone for specimens subjected to longer fire duration. The widths and lengths of the cracks were also smaller in fire-exposed specimens, indicating the larger hinging zone triggered by fire exposure (Fig. A.5 and A.6). Realistic determination of potential plastic hinge lengths of reinforced precast concrete columns is of vital importance for the postfire seismic performance assessment of existing buildings. The ratio of the plastic hinge length to the height of the column decreases with an increasing shear span ratio of the reinforced precast concrete columns.[40] However, there are no studies demonstrating the effects of fire on plastic hinge length for reinforced precast concrete columns. Hence, there is a strong need for more experimental studies to clarify the plastic hinge length after fire damage.

No damage or rotation of any socket foundations of the tested columns was observed during the seismic tests, indicating that the socket foundations provided substantial fixity at the base of the precast concrete columns. Also, no cracks were observed in the grout, indicating that seismic forces were resisted through the cantilever action of the precast concrete columns resulting from the rigid column-to-foundation connection detail. Previous studies have reported similar seismic behavior of precast concrete columns with socket foundations in terms of no grout damage even when larger grout thicknesses were used.[2,41-43] As precast concrete has emerged in the building marketplace over the past decades, complying with fire resistance became a challenge for engineers in terms of respecting the prescriptive assembly descriptions of the design specifications, so testing these assemblies became the common method for approval in practical applications.[41] Therefore, the experimental research presented here serves as a basis for developing postfire seismic resistance assessment procedures for concrete assemblies that could be included in existing performance assessment guidelines. It should be noted that the present study focuses on columns of typical low-rise reinforced precast concrete structures with low axial load (that is, 10% of the axial load capacity), in which the effect of axial load on column behavior is quite limited. Therefore, fire tests in this study were conducted without axial load, which has been done by other researchers as well.[16–17]

Conclusions

Based on the experimental and analytical findings of the present study that investigated the postfire seismic behavior of four full-scale reinforced precast concrete columns, the following conclusions are drawn.

- All specimens reached their theoretical flexural yield capacity, and none of the specimens experienced shear failure or noticeable shear damage. The analytical model was in reasonable agreement with the experimental results in terms of predicting the lateral load-displacement envelope and the failure mode. This indicates that basic principles of structural mechanics are applicable to postfire seismic performance assessment when the effect of fire on material characteristics is carefully considered.

- Postfire lateral load capacities were not considerably affected by an increase in fire duration up to 60 minutes. For 90 minutes of fire exposure, a reduction in lateral load capacity of the column of approximately 10% was observed. The reduction in lateral load capacity appeared to be caused by concrete residual properties following fire exposure. Typical low axial loads in reinforced precast concrete columns were observed to limit the effects of concrete compressive strength loss on postfire seismic behavior of the columns. The reduction in lateral load capacity for the column subjected to 90 minutes of fire exposure also caused a slight reduction in the energy dissipation capacity.

- Ductility factors and lateral drift capacities of the columns were not significantly affected by fire exposure of up to 60 minutes. For the specimen subjected to 90 minutes of fire exposure, ductility reduction was about 13% with respect to the unfired column. This reduction is attributed to the nonproportional increases in the yield and ultimate displacements during the postfire seismic tests due to reduced stiffness after fire. This slight reduction in ductility can be expected for the tested reinforced precast concrete columns with a typically low compressive axial force (as in practice), symmetric reinforcement, and considerable lateral confinement.

- The plastic deformations were distributed within a height measured from the column-footing interface equal to half the depth of the column cross section for the reference specimen and the specimen with 30 minutes of fire exposure. In contrast, plastic deformations were distributed within a height approximately equal to the full depth of the column cross section during postfire seismic tests of columns heated for 60 and 90 minutes.

- The initial stiffness of the fire-damaged specimens was reduced up to approximately 33% due to the existing cracks caused by fire exposure. Initial stiffness reductions were almost proportional to the duration of the fire exposure. The reductions in stiffness values were observed to be higher than the reductions in the lateral load capac-

ities. Fire exposure had a greater effect on the residual stiffness up to yielding because the structural response is governed by concrete residual properties up to yielding, whereas after yielding, reinforcement characteristics that have been restored after cooling are more dominant.

These conclusions are based on the results from the specific tests presented in this paper. More experiments are needed to fully understand the behavior of precast concrete structures after fire exposure.

Acknowledgments

The authors wish to express their gratitude to the Scientific and Technological Research Council of Turkey (project 216M535), the Istanbul Technical University Scientific Research Department (project 39548), Yapı Merkezi Prefabrication Inc., Allianz Insurance Inc., Turk YTONG Inc., and Fibrobeton Inc. for financial and in-kind supports. Assistance of G. Unal, E. Binbir, C. Goksu, and the staff of the Turkish Standards Institution, particularly M. Calis and A.F. Kara, are also acknowledged.

References

1. Dougherty, C. 2018. "Piece by Piece, a Factory-Made Answer for a Housing Squeeze." *New York Times*, June 7, 2018. https://www.nytimes.com/2018/06/07/business/economy/modular-housing.html.

2. *fib* (International Federation for Structural Concrete). 2004. *Seismic Design of Precast Concrete Building Structures*. Bulletin 27. Lausanne, Switzerland: *fib*.

3. Brunesi, E., R. Nascimbene, D. Bolognini, and D. Bellotti. 2015. "Experimental Investigation of the Cyclic Response of Reinforced Precast Concrete Framed Structures." *PCI Journal* 60 (2): 57–79.

4. Sezen, H., and A. S. Whittaker. 2006. "Seismic Performance of Industrial Facilities Affected by the 1999 Turkey Earthquake." *Journal of Performance of Constructed Facilities* 20 (1): 28–36.

5. Scawthorn, C., J. M. Eidinger, and A. Schiff, eds. 2005. *Fire Following Earthquake*. Technical Council on Lifeline Earthquake Engineering Monograph 26. Reston, VA: American Society of Civil Engineers.

6. Bénichou, N., H. Mostafaei, M. F. Green, and K. Hollingshead. 2013. "The Impact of Fire on Seismic Resistance of Fibre Reinforced Polymer Strengthened Concrete Structural Systems." *Canadian Journal of Civil Engineering* 40 (11): 1044–1049.

7. Lie, T. T., and R. J. Irwin. 1990. "Evaluation of the Fire Resistance of Reinforced Concrete Columns with Rectangular Cross-Sections." Internal report 601. Ottawa, ON, Canada: National Research Council Canada.

8. Franssen, J. M., and J. C. Dotreppe. 2003. "Fire Tests and Calculation Methods for Circular Concrete Columns." *Fire Technology* 39 (1): 89–97.

9. Tan, K. H., and Y. Yao. 2003. "Fire Resistance of Four-Face Heated Reinforced Concrete Columns." *Journal of Structural Engineering* 129 (9): 1220–1229.

10. Bénichou, N., D. Cree, E. U. Chowdhury, M. F. Green, and L. A. Bisby. 2011. "Fire Testing of FRP Strengthened Reinforced Concrete Columns." In *International Conference on Durability and Sustainability of Fibre Reinforced Polymer (FRP) Composites for Construction and Rehabilitation: Proceedings, July 20–22, 2011, Quebec City, Canada.*

11. Khaliq, W., and V. R. Kodur. 2013. "Behavior of High Strength Fly Ash Concrete Columns under Fire Conditions." *Materials and Structures* 46 (5): 857–867.

12. Yaqub, M., C. G. Bailey, P. Nedwell, Q. U. Z. Khan, and I. Javed. 2013. "Strength and Stiffness of Post-Heated Columns Repaired with Ferrocement and Fibre Reinforced Polymer Jackets." *Composites Part B: Engineering* 44 (1): 200–211.

13. Lie, T. T., T. J. Rowe, and T. D. Lin. 1986. "Residual Strength of Fire-Exposed Reinforced Concrete Columns." In *Evaluation and Repair of Fire Damage to Concrete*, SP-092, pp. 153–174. Farmington Hills, MI: ACI (American Concrete Institute.

14. Jau, W. C., and K. L. Huang. 2008. "A Study of Reinforced Concrete Corner Columns after Fire." *Cement and Concrete Composites* 30 (7): 622–638.

15. Chen, Y. H., Y. F. Chang, G. C. Yao, and M. S. Sheu. 2009. "Experimental Research on Post-fire Behaviour of Reinforced Concrete Columns." *Fire Safety Journal* 44 (5): 741–748.

16. Yaqub, M., and C. G. Bailey. 2012. "Seismic Performance of Shear Critical Post-Heated Reinforced Concrete Square Columns Wrapped with FRP Composites." *Construction and Building Materials* 34: 457–469.

17. Bailey, C. G., and M. Yaqub. 2012. "Seismic Strengthening of Shear Critical Post-heated Circular Concrete Columns Wrapped with FRP Composite Jackets." *Composite Structures* 94 (3): 851–864.

18. Mostafaei, H., and J. K. Hum. 2010. *Response Simulation of Reinforced Concrete Columns under Lateral Loads*. IRC-RR-294. Ottawa, ON, Canada: National Research Council Canada.

19. Franssen, J. M., and T. Gernay. 2017. "Modeling Structures in Fire with SAFIR: Theoretical Background and Capabilities." *Journal of Structural Fire Engineering* 8 (3): 300–323.

20. Associated Press. 1997. "Philadelphia to Raze Site of High-Rise Fire." *New York Times*, November 14, 1997. http://www.nytimes.com/1997/11/14/us/philadelphia-to-raze-site-of-high-rise-fire.html.

21. Almand, K. H. 2013. *Structural Fire Resistance Experimental Research: Priority Needs of U.S. Industry*. New York, NY: Springer.

22. Ministry of Public Works and Settlement. 2007. *Specification for Buildings to be Built in Disaster Areas*. Ankara, Turkey: Ministry of Public Works and Settlement.

23. ISO (International Organization for Standardization) Technical Committee 92 Subcommittee 2. 1999. *Fire Resistance Tests—Elements of Building Construction—Part 1: General Requirements*. ISO 834-1:1999. Geneva, Switzerland: ISO.

24. ASTM Subcommittee E05.11. 2012. *Standard Test Methods for Fire Tests of Building Construction and Materials*. ASTM E119-12a. West Conshohocken, PA: ASTM International.

25. CEN (European Committee for Standardization) Technical Committee CEN/TC250. 2004. *Eurocode 2: Design of Concrete Structures—Part 1-2: General Rules—Structural Fire Design*. EN 1992-1-2. Brussels, Belgium: CEN.

26. Mostafaei, H., F. J. Vecchio, and N. Bénichou. 2009. *Seismic Resistance of Fire-Damaged Reinforced Concrete Columns*. NRCC-52623. Ottawa, ON, Canada: National Research Council Canada.

27. Chang, Y. F., Y. H. Chen, M. S. Sheu, and G. C. Yao. 2006. "Residual Stress–Strain Relationship for Concrete after Exposure to High Temperatures." *Cement and Concrete Research* 36 (10): 1999–2005.

28. Mander, J. B., M. J. N. Priestley, and R. Park. 1988. "Theoretical Stress-Strain Model for Confined Concrete." *Journal of Structural Engineering* 114 (8): 1804–1826.

29. Neves, I. C., J. P. C. Rodrigues, and A. D. P. Loureiro. 1996. "Mechanical Properties of Reinforcing and Prestressing Steels after Heating." *Journal of Materials in Civil Engineering* 8 (4): 189–194.

30. Chadwell, C. B., and R. A. Imbsen. 2004. "XTRACT: A Tool for Axial Force-Ultimate Curvature Interactions." In *Structures 2004: Building on the Past, Securing the Future, Proceedings, May 22–26, 2004, Nashville, Tennessee*. Reston, VA: American Society of Civil Engineers.

31. Paulay, T., and M. J. N. Priestley. 1992. *Seismic Design of Reinforced Concrete and Masonry Buildings*. New York, NY: John Wiley & Sons Inc.

32. Fischinger, M., B. Zoubek, and T. Isaković. 2014. "Seismic Response of Precast Industrial Buildings." Vol. 1 of *Perspectives on European Earthquake Engineering and Seismology*, edited by A. Ansal, 131–177. Cham, Switzerland: Springer.

33. ACI Committee 374. 2013. *Guide for Testing Reinforced Concrete Structural Elements Under Slowly Applied Simulated Seismic Loads*. ACI 374.2R-13. Farmington Hills, MI: ACI.

34. Sheikh, S. A., and S. K. Khoury. 1993. "Confined Concrete Columns with Stubs." *ACI Structural Journal* 90 (4): 414–431.

35. Iacobucci, R. D., S. A. Sheikh, and O. Bayrak. 2003. "Retrofit of Square Concrete Columns with Carbon Fiber-Reinforced Polymer for Seismic Resistance." *ACI Structural Journal* 100 (6): 785–794.

36. Memon, M. S., and S. A. Sheikh. 2005. "Seismic Resistance of Square Concrete Columns Retrofitted with Glass Fiber-Reinforced Polymer." *ACI Structural Journal* 102 (5): 774–783.

37. Sheikh, S. A., and G. Yau. 2002. "Seismic Behavior of Concrete Columns Confined with Steel and Fiber-Reinforced Polymers." *ACI Structural Journal* 99 (1): 72–80.

38. Goksu, C., H. Yilmaz, S. R. Chowdhury, K. Orakcal, and A. Ilki. 2014. "The Effect of Lap Splice Length on the Cyclic Lateral Load Behavior of RC Members with Low-Strength Concrete and Plain Bars." *Advances in Structural Engineering* 17 (5): 639–658.

39. Bae, S., and O. Bayrak. 2008. "Plastic Hinge Length of Reinforced Concrete Columns." *ACI Structural Journal* 105 (3): 290–300.

40. Fischinger, M., M. Kramar, and T. Isaković. 2008. "Cyclic Response of Slender RC Columns Typical of Precast Industrial Buildings." *Bulletin of Earthquake Engineering* 6 (3): 519–534.

41. Magliulo, G., M. Ercolino, C. Petrone, O. Coppola, and G. Manfredi. 2014. "The Emilia Earthquake: Seismic Performance of Precast Reinforced Concrete Buildings." *Earthquake Spectra* 30 (2): 891–912.

42. Skalko, S. V. 2013. "Building Codes Evolve through Experience, Research." *PCI Journal* 58 (3): 34–40.

43. Karadogan, F., E. Yuksel, A. Ilki, H. Saruhan, K. Darilmaz, and O. Guzel. 1997. "Seismic Behavior of Precast RC Columns and Their Socket Base Connections." In *4th National Earthquake Engineering Conference (4UDMK), Ankara, Turkey*. Istanbul, Turkey: Turkish Chamber of Civil Engineers.

Notation

A_{cc} = area of concrete core section

A_g = gross cross-sectional area

A_o = area of lateral reinforcement

A_s = area of longitudinal steel reinforcement

c = specific heat

d_c = concrete core dimension to center line of the perimeter tie

f_c' = compressive strength of concrete at ambient temperature

f_{cT}' = residual compressive strength of concrete after fire exposure

f_{max} = maximum tensile stress

f_u = ultimate tensile stress

f_y = yield stress

h = depth of the cross section

h_c = convective heat flux between gas and solid

h_{cc} = coefficient of convection

h_r = radiative heat flux emitted by a solid

i = cycle number

k = thermal conductivity

K = secant stiffness

K_i = secant stiffness at cycle i

l = shear span

l_p = plastic hinge length

M = moment

n = axial load ratio

N = applied axial load

N_0 = axial load capacity

P = lateral load

P_i = lateral load at cycle i

P_{max} = maximum lateral load

Q = constant for internal generation of heat

r = residual plastic displacement ratio

s = spacing of the lateral reinforcement

t = time

T = temperature

T_g = temperature of the gas

T_s = temperature at the surface of the solid

x = vector of Cartesian coordinates

y = vector of Cartesian coordinates

z = vector of Cartesian coordinates

Δ = lateral displacement

Δ_i = lateral displacement at cycle i

Δ_p = lateral plastic displacement

Δ_{res} = residual lateral plastic displacement when the lateral load is zero

Δ_u = lateral ultimate displacement

Δ_{un} = specified peak displacement for each drift ratio

Δ_y = lateral yield displacement

ε = emissivity of the solid

ε_c = compressive strain of unconfined concrete

ε_{cc} = compressive strain of confined concrete

ε_{max} = maximum tensile strain

ε_o = peak compressive strain of concrete at ambient temperature

ε_{oT} = residual peak compressive strain of concrete after fire exposure

ε_s = tensile strain of longitudinal steel reinforcement

ε_y = yield strain

ε_u = ultimate tensile strain

θ_p = plastic rotation

μ_Δ = ductility factor

ρ = specific mass

ρ_l = ratio of longitudinal steel reinforcement

ρ_t = ratio of lateral reinforcement

σ = Stefan-Boltzmann constant

ϕ = curvature

ϕ_p = plastic curvature

ϕ_y = yield curvature

About the authors

Ugur Demir, PhD, is a research and teaching assistant in the Civil Engineering Department of Hakkari University in Hakkari, Turkey. His research interests include postfire seismic performance, retrofitting, and structural health monitoring of reinforced concrete structures.

Mark Green, PhD, is a professor of civil engineering and vice dean of the Faculty of Engineering and Applied Science at Queen's University at Kingston, ON, Canada. He is interested in the structural fire performance of concrete structures, applications of fiber-reinforced polymers in structures, the effects of cold regions on concrete structures, and monitoring of structures. The dynamics of bridge structures and the performance of bridge expansion joints are also topics of interest.

Alper Ilki, PhD, is a professor at Istanbul Technical University in Istanbul, Turkey. He is interested in the assessment of the seismic performance of reinforced concrete and masonry structures, seismic retrofitting, and applications of fiber-reinforced polymers in structures.

Abstract

Quantifying the seismic resistance of reinforced concrete buildings after fire is difficult because of the lack of information regarding their strength and ductility under earthquake loads. In this study, four full-scale flexure-controlled reinforced precast concrete columns were subjected to quasi-static reversed cyclic lateral loading under constant axial load to examine the seismic response of reinforced precast concrete columns damaged by 30, 60, and 90 minutes of fire. For the first time, the impact of fire damage on force-displacement behavior, moment-curvature relationship, stiffness, energy dissipation capacity, and residual displacements was investigated through postfire seismic tests. Test results clearly indicated that the fire exposure did not significantly affect the lateral-load-bearing capacity, failure modes, and ductility of the columns, with the exception of the specimen subjected to 90 minutes of fire exposure. The analytical study consisting of thermal and fiber-based structural analysis demonstrated that conventional principles of structural mechanics are valid for estimation of the postfire seismic behavior of reinforced precast concrete columns when the deteriorations in materials are realistically taken into account and the given algorithm is followed.

Keywords

Column, ductility, fire, lateral load capacity, reinforced concrete, seismic.

Review policy

This paper was reviewed in accordance with the Precast/Prestressed Concrete Institute's peer-review process.

Reader comments

Please address any reader comments to *PCI Journal* editor-in-chief Tom Klemens at tklemens@pci.org or Precast/Prestressed Concrete Institute, c/o *PCI Journal*, 8770 W. Bryn Mawr Ave., Suite 1150, Chicago, IL 60631.